

Fourier transform detection of weak optical transitions with cyclic routines

Jesse S. Schelfhout, Lilani D. Toms-Hardman and John J. McFerran^{1, a)}

Department of Physics, University of Western Australia, 35 Stirling Highway, 6009 Crawley, Australia

(Dated: 26 October 2020)

We demonstrate a means of detecting weak optical transitions in cold atoms that undergo cyclic routines with high sensitivity. The gain in sensitivity is made by probing atoms on alternate cycles leading to a regular modulation of the ground state atom population when at the resonance frequency. The atomic transition is identified by conducting a fast Fourier transform via algorithm or instrument. We find an enhancement of detection sensitivity compared to more conventional scanning methods of ~ 20 for the same sampling time, and can detect clock lines with fewer than 10^3 atoms in a magneto-optical trap. We apply the method to the $(6s^2) ^1S_0 - (6s6p) ^3P_0$ clock transition in ^{171}Yb and ^{173}Yb . The ac-Stark shift of this line in ^{171}Yb is measured to be $0.19(3) \text{ kHz} \cdot \text{W}^{-1} \cdot \text{m}^2$ at 556 nm.

We investigate a technique of detecting weakly allowed optical transitions that have poor signal-to-noise ratio (SNR) when using conventional frequency sweep methods. This is of importance given the resurgence of isotopic shift spectroscopy used to search for beyond Standard-Model signatures^{1–3}. Forbidden transitions in neutral atoms, such as the $^1S_0 - ^3P_0$ transition in group-II-like atoms^{4,5} may be used in such investigations. Knowledge of isotopic shifts is also relevant to many radiopharmaceutical applications^{6–8}. We demonstrate a means to increase the sensitivity of detecting weak transitions and apply it to the clock transition in the composite fermions of ytterbium^{9,10}. The method is applicable to any transition in atoms that undergo cyclic preparation before probing. With regard to searching for atomic transitions, the technique is appropriate where the ratio of search space in frequency, Δf_S , to transition linewidth, $\Delta \nu$, is not excessively large. For example, where the transition frequency can be estimated using the knowledge of isotope shifts¹¹, or in the case of photoassociation spectroscopy, estimated using a Le Roy–Bernstein type equation^{12,13}. The gain in detection sensitivity is made by cycling the probe light and looking for a corresponding signal in the Fourier domain. For example, if we refer to each atom loading and cooling cycle as one cycle, then for subsequent cycles the probe light alternates between on and off. When on resonance, some fraction of atoms will be excited to the upper state every second cycle. This appears as a modulation of the fluorescence received by the photodetector, which is proportional to the number of atoms in the ground state. The strength of the modulation is extracted through the FFT of a time record of the photoreceiver’s signal. We demonstrate the sensitivity of the method by performing spectroscopy on the $^1S_0 - ^3P_0$ line in ^{171}Yb and ^{173}Yb , which have natural linewidths of approximately 40 mHz¹⁴. A Fourier signal with ~ 10 dB SNR is observed for the ^{171}Yb clock line with $\sim 10^3$ atoms. We note that the technique should be well suited to searching for clock transitions in bosonic isotopes when held in an optical lattice

trap^{15–17}. It could also be applied in the search for photoassociation resonances in ultra cold molecules^{18–21}, for example, at predicted frequencies, where otherwise they are not apparent²².

The experiment is comprised of a magneto-optical trap (MOT), a frequency comb (MenloSystems FC1500), a hydrogen maser (KVARZ-75A), cooling lasers at 399 nm and 556 nm, and the clock-line laser at 578 nm to probe the $^1S_0 - ^3P_0$ transition. The main components are shown in Fig. 1. The source of ytterbium atoms is provided by an oven at $\sim 400^\circ\text{C}$ from which atoms effuse through an array of narrow collimation tubes orientated horizontally. Some fraction of atoms

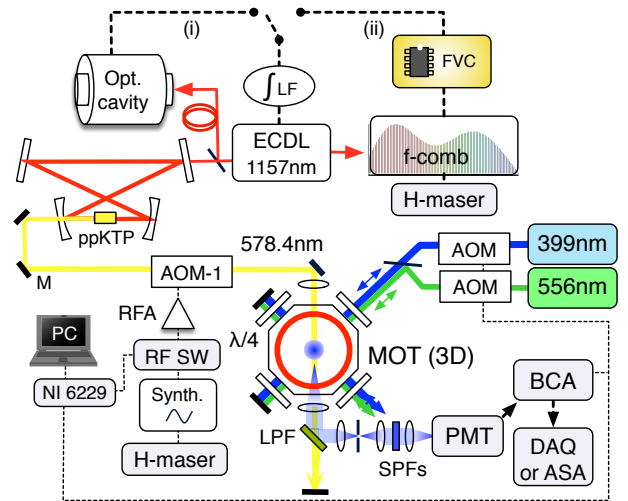


FIG. 1. An outline of the experimental layout for the $^1S_0 - ^3P_0$ line spectroscopy in Yb. (i) and (ii) represent two means of stabilizing the 1157 nm laser. AOM, acousto-optic modulator; ASA, audio (FFT) spectrum analyser; BCA, boxcar averager; ECDL, extended cavity diode laser; f-comb, frequency comb (in the near-IR); FVC, frequency-to-voltage converter; H, hydrogen; LPF, long-wavelength pass filter; MOT, magneto-optical trap; NI, National Instruments unit; PMT, photo-multiplier tube; ppKTP, periodically poled potassium titanyl phosphate; RFA, RF amplifier; SPF, short-wavelength pass filter; SW, switch.

^{a)}Electronic mail: john.mcferran@uwa.edu.au

pass through a narrow conduit downstream that separates the vacuum chamber into two main sections: (i) the oven and (ii) the Zeeman slower and main chamber.

The MOT operates in two stages; first with 399 nm light acting on the $^1S_0 - ^1P_1$ transition, then 556 nm light acting on the $^1S_0 - ^3P_1$ transition to reduce the atomic temperature to $\sim 50 \mu\text{K}$ ²³. A dual tapered Zeeman slower (crossing zero magnetic field) assists with loading atoms into the MOT. The 399 nm light is generated by frequency doubling 798 nm light from a Ti:sapphire laser in a resonant cavity. The 556 nm light is produced by use of a second frequency doubling cavity, where the incident 1112 nm light originates from a fibre laser (NKT Photonics) that injection locks a semiconductor laser (EYP-RWL-1120). The 399 nm light is stabilized by locking to the $^1S_0 - ^1P_1$ line in atoms progressing to the Zeeman slower. The 556 nm light is stabilized by locking the sub-harmonic at 1112 nm to a mode of the frequency comb via a frequency-to-voltage converter (FVC)²⁴. The cooling laser signals are controlled with acousto-optic modulators (AOMs) driven with amplified RF signals from voltage controlled oscillators (VCOs).

The clock line laser at 578 nm is produced by use of a third frequency doubling cavity, where the master laser is an extended cavity diode laser (LD1001 Time-Base) and Hänsch-Couillaud frequency stabilization is used with the doubling cavity²⁵. The yellow light frequency is tuned with an additional AOM (AOM-1 in Fig. 1) whose RF is set with a synthesizer (Agilent E4428c) that is referenced to the H-maser (with accuracy in the 10^{-12} range).

The optical frequency of the 578 nm light is evaluated with

$$\nu = 2(nf_R - f_O \pm f_B) + f_{\text{aom}} \quad (1)$$

where f_R and f_O are the frequency comb's mode spacing and offset frequency, respectively ($f_O = 20$ MHz), f_B is the beat frequency, n is the mode number of the comb, and f_{aom} is the RF drive frequency of the AOM in the path of the 578 nm light. The sign of f_B may vary depending on the isotope. The comb's repetition rate is controlled by mixing its fourth harmonic with a ~ 1.00 GHz signal that is the sum of ~ 20 MHz and 980.0 MHz signals provided by a direct digital synthesizer (DDS) and a dielectric resonator oscillator (DRO), respectively. Hence $f_R = (f_{\text{DDS}} + f_{\text{DRO}})/4$. Both the DRO and DDS are locked to a 10 MHz signal from the H-maser. The DDS frequency is imposed by that of the 556 nm cooling light.

For the ^{171}Yb clock transition the 1157 nm laser can be stabilized in one of two ways (summarized in Fig. 1): (i) with use of an ultrastable cavity and Pound-Drever-Hall lock, or (ii) by locking to the frequency comb using the FVC technique. The ultrastable cavity (Stable Laser Systems) and laser frequency stabilization have been described previously²⁵. The coefficient of thermal expansion is zero at 29.7(2) °C, and the second order thermal expansion coefficient is $6.6 \times 10^{-10} \text{ K}^{-2}$ (for $\nu = 259.1$ THz). The laser when locked to the cavity

drifts at a rate of $20.3 \text{ mHz}\cdot\text{s}^{-1}$. The free spectral range of the cavity is 1496.5210(1) MHz. This is found by measuring the frequency separation between consecutive modes of the cavity with the frequency comb and the 1157 nm beat signal. A more accurate determination is then found using the ^{171}Yb clock transition frequency. By locking to the 173167th mode of the cavity and offsetting the 578 nm light by -284.5 MHz with AOM-1 the $^1S_0 - ^3P_0$ transition frequency can be reached. The $^1S_0 - ^3P_0$ transition for ^{173}Yb lies approximately midway between cavity modes, which makes frequency offsetting with AOMs difficult. To overcome this obstacle one could use offset sideband locking with the ultrastable cavity²⁶. Instead, our approach is to lock the 1157 nm laser to the frequency comb, which also gives flexibility in reaching the $^1S_0 - ^3P_0$ transition (rather than using a sequence of AOMs). There are some constraints because the comb is also used to stabilize the 556 nm light frequency, and beat signals can only lie at frequencies set by the bandpass filters; here, 21 MHz and 30 MHz for the 1112 nm and 1157 nm beats, respectively.

The setup for the probe laser frequency stabilization by use of a FVC (Analog Devices AD652) is shown in Fig. 2. After filtering and amplifying the beat signal from the avalanche photodiode it is divided in frequency by 128 with a prescaler (Fujitsu MB506). A comparator (LM360) regularizes the waveform making it suitable for the CMOS compatible FVC. The AD652 is a synchronous VFC, implying that its transfer function is governed by an external clock, in this case an OCXO at 10 MHz, divided by 4. A laser servo based on this scheme has been shown to produce a fractional frequency instability of $\sim 7 \times 10^{-14}$ for $0.2 < \tau < 10^3$ s, where τ is the integration time²⁴. Apart from the flexibility provided by locking to the comb, the FVC-comb lock is also extremely robust.

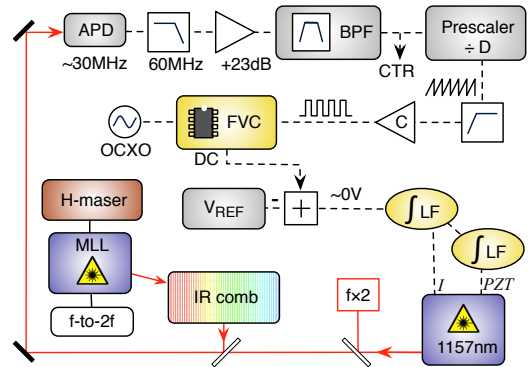


FIG. 2. Laser frequency stabilization of the probe laser by use of a frequency-to-voltage converter. In the prescaler the frequency division is $D = 128$. APD, avalanche photodiode; BPF, band pass filter; C, comparator; CTR, frequency counter; LF, loop filter (integrator); MLL, mode-locked laser; OCXO, oven controlled crystal oscillator. PZT and I represent electronic feedback to a piezo transducer and laser current, respectively.

The event sequence is presented in Fig. 3. Each cycle has a duration of 0.5 s, the majority of which is used to load atoms

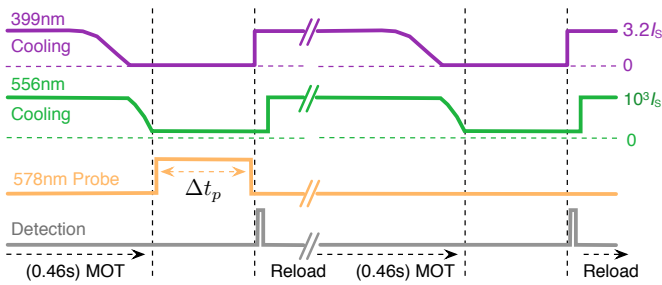


FIG. 3. Event sequence for the light fields. The 578 nm probe remains off every second cycle. The duration $\Delta t_p = 40$ ms. The saturation intensities are $I_S^{(399)} = 595 \text{ W m}^{-2}$ and $I_S^{(556)} = 1.4 \text{ W m}^{-2}$ for the $^1S_0 - ^1P_1$ and $^1S_0 - ^3P_1$ transitions, respectively. The frequency detuning of the cooling lasers is also varied to optimize signal level.

into the MOT. The 399 nm light is ramped down over 20 ms during which time the second stage cooling with 556 nm light takes effect. The 556 nm intensity is also ramped down to reduce the temperature of the atoms and minimize the ac Stark shift. The magnetic quadrupole field is held fixed with a z -axis gradient of $0.42 \text{ T}\cdot\text{m}^{-1}$. The yellow 578 nm light pulse has a period of 40 ms to interact with the atoms, after which the 399 nm is switched back on and detection of the ground state atoms is made (and MOT loading recommences). Unless otherwise stated, the maximum intensity of the 578 nm light was $5 \text{ kW}\cdot\text{m}^{-2}$ with a corresponding Rabi frequency, Ω_R , of $\sim 4 \text{ kHz}$ (representing $\sim 1/50^{\text{th}}$ of the transition linewidth). A 1 Hz modulation in the population transfer arises by applying the 578 nm light every second cycle. Fluorescence at 399 nm is filtered both spatially and spectrally before detection with a photomultiplier tube (PMT, Hamamatsu H10492-001)²⁷. The PMT signal is received by a boxcar averager (BCA, SRS SR250), which outputs to an Agilent 34970A unit for data acquisition. The BCA is triggered by the main control sequence program so that detection is made within $300 \mu\text{s}$ of the 399 nm light resuming. A single measurement involves logging N samples of the BCA output every 0.25 s, such that the total acquisition time gives an integer number of modulation cycles. A FFT of the time record (with Igor Pro software) reveals a signal at the modulation frequency if the probe laser frequency is on resonance. The upper panel of Fig. 4 shows examples of FFTs (magnitude squared) for the (a) ^{171}Yb and (b) ^{173}Yb clock transitions, where $N = 500$ in both cases (over 125 s). These are maximum strength signals recorded very close to line center. The SNR at the 1 Hz modulation is approximately 6×10^3 for ^{171}Yb and just under 2×10^3 for ^{173}Yb (we will denote this $\text{SNR}_{\text{fft,or}}$ – ‘or’ for on-resonance). The number of atoms in the 556 nm MOT generating the signal was $\sim 5 \times 10^5$ and $\sim 2 \times 10^5$, respectively (the transfer fraction to 1P_0 was $\sim 30\%$). The Yb oven was deliberately set at a relatively low temperature of 380°C . In an alternative means of obtaining the spectrum, the BCA output was sent to a FFT

spectrum analyser (HP89410A) set with a resolution bandwidth of 10 mHz and a Hanning window. The lower panel of Fig. 4 shows the resultant spectra. Figures 4(c) and 4(d) are for ^{171}Yb and ^{173}Yb , respectively. In (d) the oven was at a higher temperature of 410°C . The SNRs at 1 Hz are consistent with those in the upper panel. The signals at 0.61 Hz and 1.38 Hz are unrelated to the 578 nm light. The 1.38 Hz modulation appears to originate from the Ti:sapphire laser and the 0.61 Hz is the same modulation shifted in frequency through aliasing.

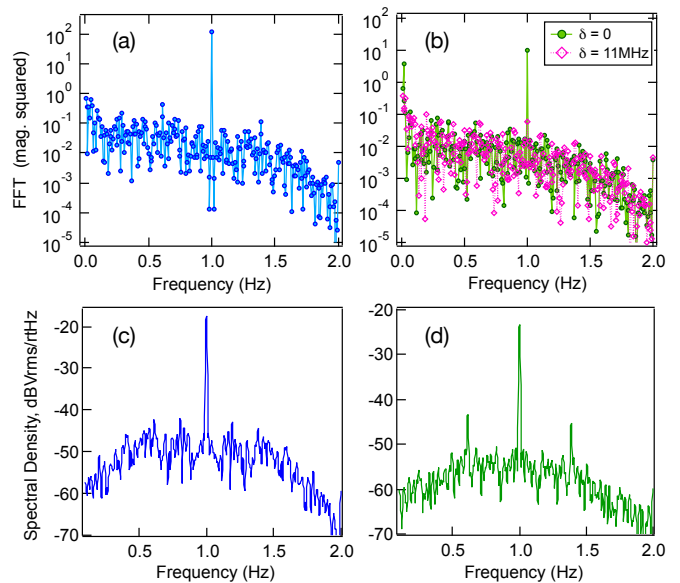


FIG. 4. Upper panel: Fast Fourier transforms of the BCA output when the 578 nm light is near the center of resonance for (a) ^{171}Yb , and (b) ^{173}Yb (circles). Lower panel: equivalent spectra recorded with an FFT spectrum analyser for (c) ^{171}Yb , and (d) ^{173}Yb . Plot (b) also shows the FFT when the 578nm light is offset from resonance by 11 MHz (diamonds).

A full line spectrum of the $^1S_0 - ^3P_0$ transition is produced by stepping the frequency of AOM-1 (with a fixed frequency for each time record) and extracting the SNR from the FFTs. Figures 5(a) and 5(b) show the $^1S_0 - ^3P_0$ line spectra for the ^{171}Yb and ^{173}Yb , respectively. Each data point is determined from a separate FFT. Figure 5(a) is shown with a logarithmic scale to illustrate the sensitivity in the wings of the profile. The absolute frequency is determined from Eq. 1. The frequencies subtracted from the line centers are $\nu_{171} = 518295836590.9 \text{ kHz}$ ³⁰ and $\nu_{173} = 518294576847.6 \text{ kHz}$ ⁹. The inset of Fig. 5(a) shows the spectrum by use of a conventional frequency sweep for ^{171}Yb with a similar number of atoms. In this case the 578 nm pulse is applied every cycle of the event sequence, unlike in Fig. 3. Here the total sampling time was 140 s with the BCA set to 3-sample averaging. Note, the noise here is not white frequency noise.

To compare the detection sensitivity of the two methods we introduce a sensitivity index $d' = (\mu_s - \mu_n) / \sigma_n$, where μ_s is

the mean of the signal level, μ_n is the mean of the noise level, and σ_n is the standard deviation of the noise²⁸. Here μ_s corresponds to the on-resonance signal. For the FFT approach the units are magnitude-squared, therefore, $d'_{\text{fft}} = \sqrt{(SNR'_{\text{fft,or}})}$. In the case of the conventional sweep we obtain $d'_{\text{swp}} = 3.3$, hence $d'_{\text{fft,or}}/d'_{\text{swp}} \approx 23$; or in power units, the gain in sensitivity is ~ 27 dB. Hence the means of detecting the transition over similar time scales is very much enhanced through the FFT approach.

The spectra in Figs. 5(a) and Fig. 5(b) have their own SNR. In this case we do not use the noise floor of the FFT to set the noise level. More appropriate is the rms of the residuals to the line shape fits. Here the SNR is 38 and 16 for ^{171}Yb and ^{173}Yb , respectively. The conventional scan for ^{173}Yb produced no evident transition over the 140 s of sampling, due to the lower number of atoms trapped. The total sample time for Figs. 5(a) and Fig. 5(b) was 1500 s and 1300 s, respectively, so while there is a significant gain in SNR, the total sampling time increased by ~ 10 fold. From the Lorentzian line shape

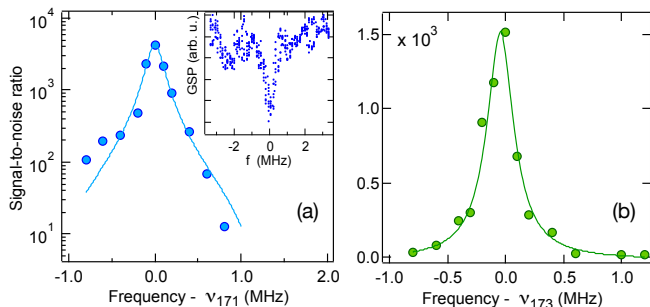


FIG. 5. SNR (magnitude squared) versus optical frequency for the $^1S_0 - ^3P_0$ line in (a) ^{171}Yb and (b) ^{173}Yb by use of the FFT and cyclic modulation. The inset shows a spectrum for ^{171}Yb with a conventional scan. GSP, ground state population.

fits (to suit the wings) the FWHM for traces (a) and (b) are 210 kHz and 290 kHz, respectively. The width for ^{171}Yb is consistent with the temperature of the atoms determined by imaging of ballistic expansion, $T \sim 50 \mu\text{K}$ ²⁷. For ^{173}Yb there may be a linewidth contribution from laser noise²⁴, since the FVC lock to the comb was used rather than the ultrastable cavity.

Figure 6(a) shows the on-resonance 1 Hz SNR versus the number of atoms contributing to the signal for ^{171}Yb with $\Omega_R = 4$ kHz and 10 kHz (varied through 578 nm intensity). The number of atoms is determined by use of $N_a = V/(h\nu G f \gamma_p)$, where V is the dc voltage from the PMT (background subtracted), h is Planck's constant, ν is the frequency of the 399 nm light, G is the gain of the PMT (V/W), f is the collected fraction of fluorescence, and γ_p is the photon scattering rate. The scattering rate follows from: $\gamma_p = s_0\gamma/(1 + s_0 + (2\delta/\gamma)^2)/2$, where s_0 is the 399 nm intensity normalized by the saturation intensity, $I_S^{(399)}$, δ is the frequency detuning

and γ is the natural linewidth of the $^1S_0 - ^1P_1$ transition²⁹. The atom number was varied by changing the current through the Zeeman slower coils. With $\sim 10^3$ atoms a Fourier signal $\gtrsim 10$ dB SNR remains apparent when $\Omega_R = 10$ kHz. The sensitivity increases with 578 nm intensity. Note, our fluorescence collection efficiency is only 0.55 %.

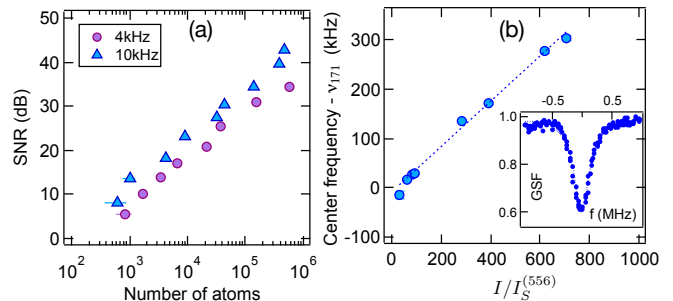


FIG. 6. (a) SNR of the 1 Hz FFT signal, on resonance, versus atom number for two values of Ω_R . (b) Frequency of the ^{171}Yb $^1S_0 - ^3P_0$ transition versus 556 nm light intensity. Inset: spectrum of the ^{171}Yb clock line after optimization. GSF, ground state fraction.

Once an atomic line is found, the modulated BCA output can aid optimization, such as improving the probe beam overlap with the atom cloud. An example of the ^{171}Yb clock line recorded with the conventional scan is shown in the inset of Fig. 6(b) after such an optimization (and $T_{\text{oven}} = 410^\circ\text{C}$). The green light intensity during the 578 nm pulse was $I/I_S^{(556)} = 140$. By repeating with different levels of 556 nm light the ac-Stark shift becomes evident, as seen in Fig. 6(b). The line center for zero light intensity is within 9 kHz of previous reports of the transition frequency^{5,30}. The gradient of the line fit for the ac-Stark shift is $0.19(3) \text{ kHz}\cdot\text{W}^{-1}\cdot\text{m}^2$, where the uncertainty is dominated by that of the light intensity.

In summary, we have demonstrated a sensitive method of detecting weak optical transitions in cold atoms that rely on cyclic routines. In terms of detecting the presence of a transition, the sensitivity index is increased 20-fold compared to conventional line scanning for similar measurement times. One can detect (and resolve) a clock transition in an optical lattice with $\sim 10^3$ atoms³¹, but to our knowledge the detection of such a transition with 10^3 atoms in a MOT has not been previously demonstrated. With regard to line spectra, the increased SNR comes at the expense of a 10-fold increase in sampling time, which places a restriction on $\Delta f_S/\Delta\nu$ (mentioned in the opening). An upper limit for $\Delta f_S/\Delta\nu$ may be ~ 20 for practical purposes, but it depends on factors such as cycle time and how well search procedures can be automated.

ACKNOWLEDGMENTS

This work was supported by the Australian Research Council's grant CE170100009. J. S. acknowledges support

from the University of Western Australia’s Winthrop Scholarship, and St Catherine’s College. We thank F. van Kann and L. Nenadović for proofreading the manuscript.

DATA AVAILABILITY

The data that support the findings of this study are available from the corresponding author upon request.

REFERENCES

- ¹V. V. Flambaum, A. J. Geddes, and A. V. Viatkina, “Isotope shift, nonlinearity of King plots, and the search for new particles,” *Phys. Rev. A* **97**, 032510 (2018).
- ²I. Counts, J. Hur, D. P. L. Aude Craik, H. Jeon, C. Leung, J. C. Berengut, A. Geddes, A. Kawasaki, W. Jhe, and V. Vuletić, “Evidence for nonlinear isotope shift in Yb^+ search for new boson,” *Phys. Rev. Lett.* **125**, 123002 (2020).
- ³C. Solaro, S. Meyer, K. Fisher, J. C. Berengut, E. Fuchs, and M. Drewsen, “Improved isotope-shift-based bounds on bosons beyond the standard model through measurements of the $^2\text{D}_{3/2} - ^2\text{D}_{5/2}$ interval in Ca^+ ,” *Phys. Rev. Lett.* **125**, 123003 (2020).
- ⁴M. Takamoto, F.-L. Hong, R. Higashi, and H. Katori, “An optical lattice clock,” *Nature* **435**, 321 (2005).
- ⁵A. Ludlow, M. Boyd, J. Ye, E. Peik, and P. Schmidt, “Optical atomic clocks,” *Rev. Mod. Phys.* **87**, 637–701 (2015).
- ⁶P. T. Greenland, “Laser isotope separation,” *Contemporary Physics* **31**, 405–424 (1990).
- ⁷H. Park, D.-H. Kwon, Y. H. Cha, T.-S. Kim, J. Han, K.-H. Ko, D.-Y. Jeong, and C.-J. Kim, “Stable isotope production of ^{168}Yb and ^{176}Yb for industrial and medical applications,” *Journal of Nuclear Science and Technology* **45**, 111–116 (2008).
- ⁸U. Köster, W. Assmann, C.-O. Bacri, T. Faestermann, P. Garrett, R. Gernhäuser, and I. Tomandl, “Electromagnetic isotope separation of gadolinium isotopes for the production of $^{152,155}\text{Tb}$ for radiopharmaceutical applications,” *Nuclear Instruments and Methods in Physics Research Section B* **463**, 111 – 114 (2020).
- ⁹C. Hoyt, Z. Barber, C. Oates, T. Fortier, S. Diddams, and L. Hollberg, “Observation and absolute frequency measurements of the $^1\text{S}_0 - ^3\text{P}_0$ optical clock transition in neutral ytterbium,” *Phys. Rev. Lett.* **95**, 083003–1 (2005).
- ¹⁰N. Hinkley, J. A. Sherman, N. B. Phillips, M. Schioppo, N. D. Lemke, K. Beloy, M. Pizzocaro, C. W. Oates, and A. D. Ludlow, “An atomic clock with 10^{-18} instability,” *Science* **341**, 1215 (2013).
- ¹¹R. Zinkstok, E. J. van Duijn, S. Witte, and W. Hogervorst, “Hyperfine structure and isotope shift of transitions in Yb I using UV and deep-UV cw laser light and the angular distribution of fluorescence radiation,” *J. Phys. B* **35**, 2693–2701 (2002).
- ¹²J. Weiner, V. S. Bagnato, S. Zilio, and P. S. Julienne, “Experiments and theory in cold and ultracold collisions,” *Rev. Mod. Phys.* **71**, 1–85 (1999).
- ¹³S. Tojo, M. Kitagawa, K. Enomoto, Y. Kato, Y. Takasu, M. Kumakura, and Y. Takahashi, “High-resolution photoassociation spectroscopy of ultracold ytterbium atoms by using the intercombination transition,” *Phys. Rev. Lett.* **96**, 153201–1 (2006).
- ¹⁴S. G. Porsev and A. Derevianko, “Hyperfine quenching of the metastable $^3\text{P}_{0,2}$ states in divalent atoms,” *Phys. Rev. A* **69**, 042506 (2004).
- ¹⁵N. Poli, Z. Barber, N. Lemke, C. Oates, L. Ma, J. Stalnaker, T. Fortier, S. Diddams, L. Hollberg, J. Bergquist, A. Bruschi, S. Jefferts, T. Heavner, and T. Parker, “Frequency evaluation of the doubly forbidden $^1\text{S}_0 \rightarrow ^3\text{P}_0$ transition in bosonic ^{174}Yb ,” *Phys. Rev. A* **77**, 050501 (2008).
- ¹⁶T. Akatsuka, M. Takamoto, and H. Katori, “Three-dimensional optical lattice clock with bosonic ^{88}Sr atoms,” *Phys. Rev. A* **81**, 023402 (2010).
- ¹⁷X. Baillard, et al., “Accuracy evaluation of an optical lattice clock with bosonic atoms,” *Opt. Lett.*, **32**, 1812 (2007).
- ¹⁸M. Yasuda, T. Kishimoto, M. Takamoto, and H. Katori, “Photoassociation spectroscopy of ^{88}Sr : reconstruction of the wave function near the last node,” *Phys. Rev. A* **73**, 11403 – 1 (2006).
- ¹⁹T. Zelevinsky, M. M. Boyd, A. D. Ludlow, T. Ido, J. Ye, R. Ciurylo, P. Naidon, and P. S. Julienne, “Narrow line photoassociation in an optical lattice,” *Phys. Rev. Lett.* **96**, 203201 (2006).
- ²⁰K. M. Jones, E. Tiesinga, P. D. Lett, and P. S. Julienne, “Ultracold photoassociation spectroscopy: Long-range molecules and atomic scattering,” *Rev. Mod. Phys.* **78**, 483 (2006).
- ²¹N. Nemitz, F. Baumer, F. Munchow, S. Tassy, and A. Gorlitz, “Production of heteronuclear molecules in an electronically excited state by photoassociation in a mixture of ultracold Yb and Rb,” *Phys. Rev. A* **79**, 061403 (2009).

- ²²A. Guttridge, S. A. Hopkins, M. D. Frye, J. J. McFerran, J. M. Hutson, and S. L. Cornish, “Production of ultracold Cs*Yb molecules by photoassociation,” *Phys. Rev. A* **97**, 063414 (2018).
- ²³Lower temperature may be obtained with optimal MOT beam alignment.
- ²⁴F. C. Reynolds and J. J. McFerran, “Optical frequency stabilization with a synchronous frequency-to-voltage converter,” *Appl. Opt.* **58**, 3128–3132 (2019).
- ²⁵L. Nenadović and J. McFerran, “Clock and inter-combination line frequency separation in ^{171}Yb ,” *J. Phys. B* **49**, 065004 (2016).
- ²⁶J. I. Thorpe, K. Numata, and J. Livas, “Laser frequency stabilization and control through offset sideband locking to optical cavities,” *Opt. Express* **16**, 15980 – 90 (2008).
- ²⁷N. Kostylev, E. Ivanov, M. Tobar, and J. McFerran, “Sub-Doppler cooling of ytterbium with the $^1S_0 - ^1P_1$ transition including ^{171}Yb ($I=1/2$),” *J. Opt. Soc. Am. B* **31**, 1614 (2014).
- ²⁸T. D. Wickens, *Elementary Signal Detection Theory*, Oxford University Press (2002).
- ²⁹H. J. Metcalf and P. van der Straten, *Laser Cooling and Trapping*, Springer (1999).
- ³⁰www.bipm.org/en/publications/mises-en-pratique/standard-frequencies.html
- ³¹L. Yi, S. Mejri, J. J. McFerran, Y. Le Coq, and S. Bize, “Optical lattice trapping of ^{199}Hg and determination of the magic wavelength for the ultraviolet $^1S_0 \leftrightarrow ^3P_0$ clock transition,” *Phys. Rev. Lett.* **106**, 073005 (2011).